

ARTICLE

Received 10 Nov 2015 | Accepted 15 Apr 2016 | Published 1 Jun 2016

DOI: 10.1038/ncomms11643

OPEN

aPKC regulates apical localization of Lgl to restrict elongation of microridges in developing zebrafish epidermis

Renuka Raman¹, Indraneel Damle¹, Rahul Rote^{1,†}, Shamik Banerjee^{1,2}, Chaitanya Dingare^{1,†}
& Mahendra Sonawane¹

Epithelial cells exhibit apical membrane protrusions, which confer specific functions to epithelial tissues. Microridges are short actin protrusions that are laterally long and form a maze-like pattern in the apical domain. They are widely found on vertebrate squamous epithelia including epidermis and have functions in mucous retention, membrane storage and abrasion resistance. It is largely unknown how the formation of these laterally long actin projections is regulated. Here, we show that antagonistic interactions between aPKC and Lgl—regulators of apical and basolateral domain identity, respectively,—control the length of microridges in the zebrafish periderm, the outermost layer of the epidermis. aPKC regulates the levels of Lgl and the active form of non-muscle myosinII at the apical cortex to prevent actin polymerization-dependent precocious fusion and elongation of microridges. Our data unravels the functional significance of exclusion of Lgl from the apical domain in epithelial cells.

¹Department of Biological Sciences, Tata Institute of Fundamental Research, Colaba, Mumbai 400005, India. ²SASTRA University, Tirumalaisamudram, Thanjavur 613402, India. † Present addresses: McGill University, Montreal, Quebec, H3A 1B1 Canada (Ra.R.); Albert-Ludwig-University of Freiburg, Freiburg, Germany (C.D.). Correspondence and requests for materials should be addressed to M.S. (email: mahendras@tifr.res.in).

In amniotes, several kinds of epithelial cells exhibit apical membrane protrusions supported by the actin cytoskeleton. One of the classic examples of apical projections is microvilli in the intestine, kidney and the brain ventricles having secretory and absorptive functions. Microridges—another kind of apical actin protrusions—are widely found on vertebrate squamous epithelia such as epidermis, cornea, oral mucosa, vaginal epithelium and urinary bladder^{1–3}. Unlike microvilli, which are tall-cylindrical projections, microridges are short but laterally long structures, forming a labyrinth in the apical domain. The proposed function of microridges include mucous retention, membrane storage and abrasion resistance^{4,5}. It is largely unknown how microridges are formed and whether their formation is under the control of mechanisms that regulate cell polarity in the epithelial cells.

Cell polarity along the apical-basal axis is regulated by four major complexes, Par3-Par6-aPKC, Crumbs-Stardust-PatJ, Lgl-Dlg-Scrib and Yurt-Coracle-NrxIV, which are highly conserved across phyla^{6,7}. In epithelial cells and in neuroblasts, Par3-Par6-aPKC complex is localized to the apical domain, whereas Lgl-Dlg-Scrib complex is localized to the basolateral domain^{6,8–10}. In *Drosophila* epithelia, loss-of-function analyses of the Par3-Par6-aPKC complex results in a loss of apical membrane identity, mislocalization of basolateral membrane markers, failure to assemble adherens and septate junctions and loss of epithelial organization^{11–16}. Atypical protein kinase C (aPKC), a serine/threonine kinase localized at the apical domain, contributes towards the maintenance of apical identity by phosphorylation and removal of Lgl from the apical domain¹⁶. The loss of aPKC function results in loss of apical membrane identity as basolateral components mislocalize to the apical domain^{9,15,17}. The apical aPKC and basolateral Lgl thus act antagonistically to regulate many aspects of epithelial cell polarity and asymmetric division of neuroblasts^{9,15,16,18,19}.

Vertebrates have two paralogues of *lgl*, namely *lgl1* and *lgl2*. In mice, *lgl1* function is essential for the maintenance of cell polarity in the neuroepithelial cells²⁰, whereas *lgl2* functions in precise branching morphogenesis during placental development²¹. In zebrafish, *penner/lgl2* function is necessary for the formation of hemidesmosomes and to prevent hyperplasia of the basal epidermis^{22–24}. Lgl has been proposed to execute its cellular functions by regulating polarized exocytosis or by actomyosin-based mechanism^{25–27}. *Drosophila* Lgl as well as vertebrate Lgl1 physically interact with non-muscle myosinII (NMII)^{8,28–30}, which is an actin-based motor protein. The formation of a complex between NMII and Lgl depends on Lgl's phosphorylation status, which is regulated by aPKC^{31–33}. In epithelial cells, Lgl regulated NMII activity controls actomyosin contractility during early stages of cell–cell contact formation and planar polarization^{34,35}. Furthermore, in migrating cells, Lgl is known to regulate the localization of NMII and focal adhesion morphology to optimize cell migration and promote protrusion formation^{30,32}.

So far, it has remained unclear whether the elimination of Lgl from the apical domain by aPKC has any functional consequence in vertebrate epithelia. We show that the aPKC λ function is critical in restricting the length of microridges, whereas Lgl promotes their elongation. Our study points to a novel and unknown functional antagonism between Lgl and aPKC λ in regulation of apical F-actin protrusions in the vertebrate epidermis. Mechanistically, aPKC regulates levels of Lgl and active NMII at the apical cortex to inhibit actin polymerization-dependent precocious fusion and elongation of microridges. Our analyses unravel the functional significance of removal of Lgl by aPKC at the apical domain in vertebrate epithelial cells. We propose that the formation of apical projections is under regulation of the mechanisms that control cell polarization.

Results

aPKC prevents precocious elongation of apical microridges. In vertebrates, there are two aPKC isoforms namely aPKC $\lambda/1$ and aPKC ζ . The *apkc $\lambda/1$* mutant in zebrafish, *heart and soul (has)*, shows defects in the morphogenesis of retina, neural tube and intestine due to improper formation and maintenance of adherens junctions³⁶. We found that aPKC localizes to the apical domain of peridermal cells at 48 h post fertilization (hpf) (Fig. 1a; Supplementary Fig. 1a). Pearson's coefficient as well as Manders' overlap coefficient revealed substantial colocalization between aPKC and F-actin at the apical microridges. For this analysis, we used E-cadherin localization with apical F-actin as a negative control and Ezrin localization with F-actin as a positive control (Fig. 1b; Supplementary Fig. 1b,d). This apical localization of aPKC is diminished in *has/apkc $\lambda/1$* mutants as well as in *apkc $\lambda/1$* morphants (*apkc* MO)³⁶ and resulted in longer and fewer microridges (Fig. 1a; Supplementary Fig. 1c,e). Such long microridges appear in the wild-type peridermal cells only after 72 hpf suggesting their precocious elongation in aPKC $\lambda/1$ deficient embryos (henceforth called just *apkc* or aPKC). E-cadherin and ZO1 staining revealed that there was no effect on formation or localization of adherens and tight junctions in the periderm of *has/apkc* mutants (Supplementary Fig. 1f). To test whether microridges in the *has/apkc* mutants become long to accommodate excess apical membrane, the *has/apkc* mutant line was crossed to the Tg(*cldnB:lynEGFP*) line³⁷ to visualize the cell membrane of peridermal cells. Quantification of the apical as well as total surface area of peridermal cells did not reveal significant difference between the *has/apkc* mutant and wild-type siblings (Fig. 1c). Thus, increased microridge length in *has/apkc* mutants is not a consequence of increased apical surface area or impaired cell junction formation.

To gain insights into how microridges elongate over time, they were imaged in developing wild-type and aPKC-deficient embryos (Fig. 1f). Since knockdown of *apkc* recapitulates the microridge phenotype (Supplementary Fig. 1c), an antisense morpholino was used for this analysis³⁶. From embryos stained for F-actin, the microridge number and microridge perimeter was quantified. The perimeter is governed by the length in the absence of appreciable changes in the microridge width. For the sake of simplicity, perimeter is referred to as ridge length in the text and all the figures. The visualization of data by bean plot and the analysis of medians revealed that though the ridges tend to be slightly shorter at 18 hpf, there is significant shift in the length distribution towards longer ridges from 24 hpf onwards in aPKC-deficient embryos as compared with wild-type embryos (Fig. 1d). Consistently, the frequency distribution analysis revealed that while the number of short ridges decreases, the number of ridges having perimeter length above 5 μ m increases in *apkc* morphants during development (Fig. 1e). As compared with control, the total number of ridges is significantly lower in aPKC-deficient embryos (Supplementary Fig. 1e). This decrease in total number of ridges in the *apkc* morphant indicated that the shorter ridges fuse to form long ridges. To test this, we performed time-lapse imaging of peridermal cells expressing LifeActRFP³⁸. Under given live imaging conditions, we did not observe appreciable increase in microridge length till 27 hpf in the wild-type embryo (Fig. 1g, Supplementary Videos 1 and 2). The length of microridges starts to increase effectively from 27 hpf onwards due to increase in effective fusion events (Fig. 1g; Supplementary Videos 3 and 4). Intriguingly, microridge length starts to increase precociously in *apkc* morphants from 20 to 22 hpf onwards by fusion of smaller microridges. These microridges continue to stay long but are dynamic at later time points (Fig. 1g; Supplementary Videos 5–8). Movies with higher temporal resolution at 21 hpf indicate that microridges appear as

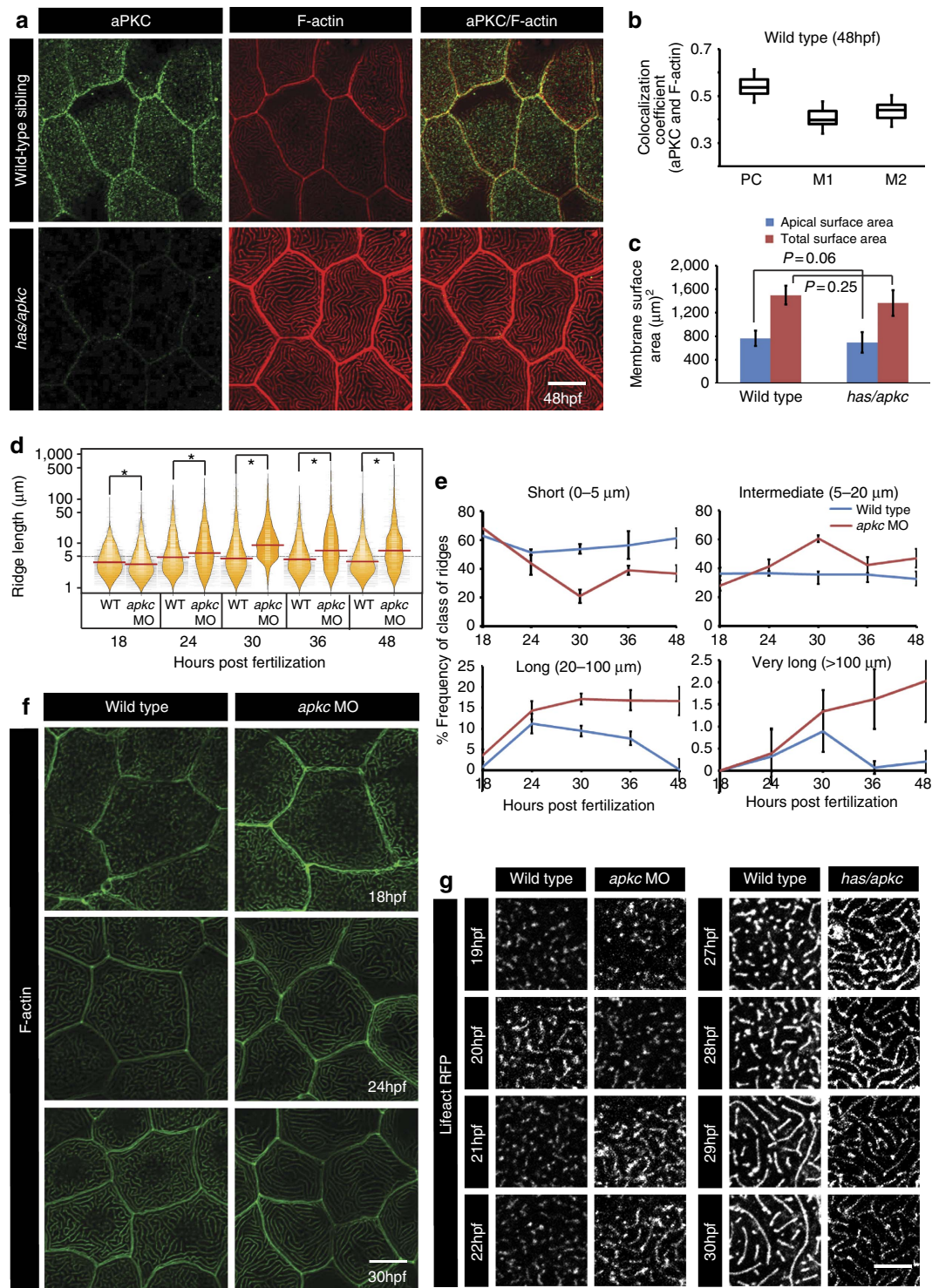


Figure 1 | *has/apkc* function is important for restricting the length of microridges by preventing their precocious elongation. Immunocolocalization using anti-aPKC antibody and phalloidin, which labels F-actin, in wild type and *has/apkc* mutant at 48 hpf (**a**) followed by colocalization coefficient analysis by Pearson's (PC) method and Manders' overlap for aPKC with F-actin (M1) and F-actin with aPKC (M2) at 48 hpf in wild-type embryos (**b**). Graphical representation (**c**) of apical surface area and total cell surface area in wild type and *has/apkc* mutant at 48 hpf. Visualization of the distribution of ridge lengths and medians in wild-type and aPKC-deficient embryos at various developmental time points using bean plots (**d**). The frequency distribution of ridges (**e**) in short (0–5 μm), intermediate (5–20 μm), long (20–100 μm) and very long (>100 μm) categories during development. Quantification in **d** and **e** are based on phalloidin stainings performed in wild-type and *apkc* morphants (**f**). Time-lapse imaging of microridges in clones expressing lifeActRFP under CMV promoter in wild-type and *apkc* morphants during 19–22 hpf and in *has/apkc* siblings (wild type) and mutants during 27–30 hpf (**g**). Error bars in **c** and **e** indicate s.d., whereas square brackets represent comparison. Probability values 'P' are for the Student's *t*-test. Asterisks in the bean plot (**d**) represent significant difference in median values at $P < 0.05$ as calculated by pairwise multiple comparison procedures using Dunn's Method. Scale bars in **a**, **f** and **g** correspond to 10 μm .

punctae in wild-type epidermal cells which do not undergo elongation, whereas microridges fuse to form longer ridges in the *apkc* morphant (Supplementary Videos 9–12).

To conclude, aPKC restricts the length of apical microridges in the peridermal cells of the zebrafish epidermis during development.

aPKC controls apical localization of Lgl in the periderm. In polarized cells, Lgl is localized to the basolateral domain where it is required for establishing domain identity^{8,26,39}. This exclusive basolateral localization of Lgl is achieved by selective removal of Lgl from the apical domain by its phosphorylation by aPKC^{8,40,41}. Therefore, we asked whether Lgl localization is altered in the peridermal cells of the *has/apkc* mutant embryos. Immuno-localization studies using anti-Lgl2 antibody revealed that at 48 hpf a minor fraction of Lgl localizes to the apical domain in wild-type, while *has/apkc* mutants exhibit slightly higher apical localization (Fig. 2a). At the apical domain, Lgl

co-localizes with F-actin at the microridges in wild-type embryos (Fig. 2b). Pearson and Manders' coefficient analysis confirmed that this colocalization is significantly higher in *has/apkc* mutants as compared with wild-type embryos (Fig. 2b,c). Temporal analysis indicated that Lgl localizes to the microridges at 24 hpf in both wild-type and aPKC-deficient embryos (Supplementary Fig. 2a). As development progresses, a minor fraction of Lgl is retained at the microridges in wild-type embryos, whereas Lgl levels increase in *has/apkc* mutants, suggesting that aPKC function is essential for controlling the levels of apical Lgl in the peridermal cells (Supplementary Fig. 2b).

Lgl promotes elongation of microridges in the apical domain.

We asked whether *lgl1* or *lgl2* function is essential for the elongation of microridges in the periderm of wild type or *has/apkc* mutant embryos. To perform the loss-of-function analysis, we used previously published *lgl1* morpholinos^{42,43} or *penner* (*pen*)/*lgl2* mutant²². Rescue experiments revealed that the

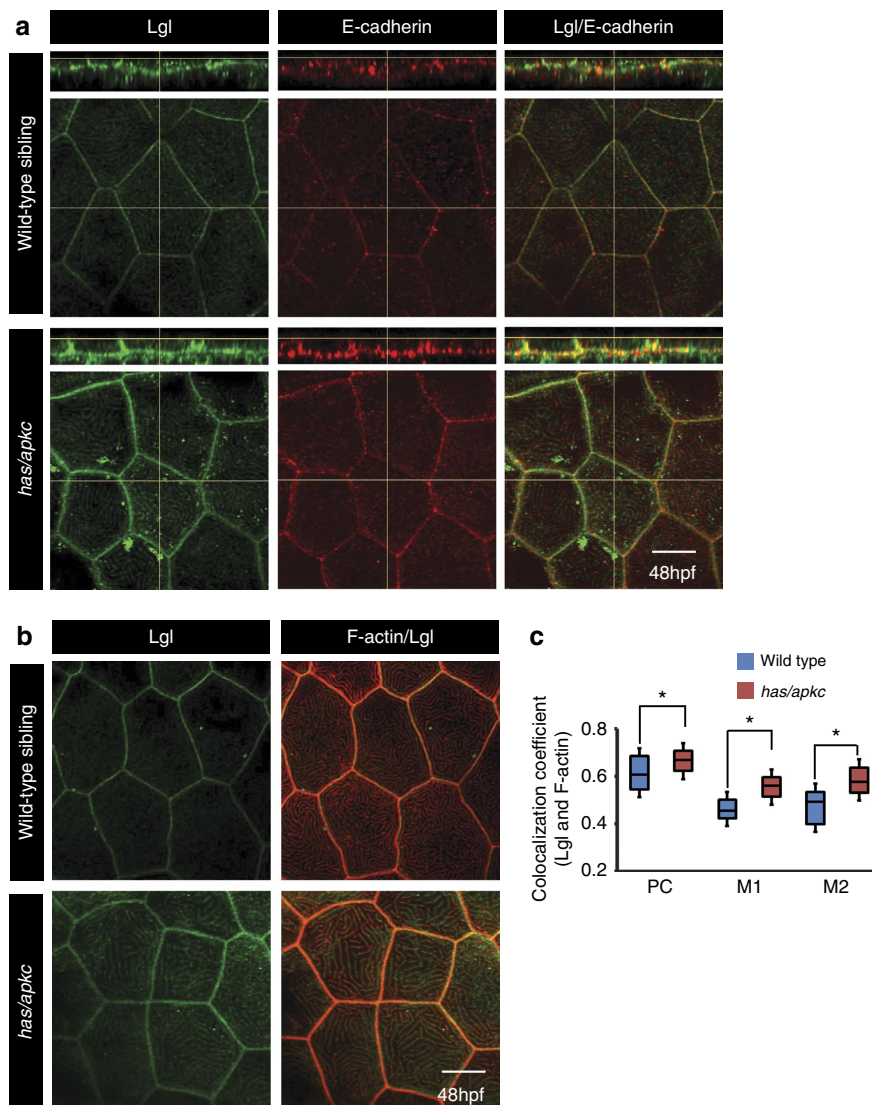


Figure 2 | The levels of apical Lgl increase in the apical domain of the head peridermal cells in *has/apkc* mutants. Immunostaining using anti-Lgl2 and E-cadherin antibodies (a) in wild-type and *has/apkc* mutant embryos. Immuno-colocalization of Lgl and F-actin in the apical domain of wild-type and *has/apkc* mutant embryos at 48 hpf (b). Colocalization coefficient analysis between Lgl and F-actin by Pearson's (PC) method and Manders' overlap for Lgl with F-actin (M1) and F-actin with Lgl (M2) at 48 hpf in wild-type and *has/apkc* mutant embryos (c). Asterisks in c indicate significant difference at $P < 0.001$ by Student's *t*-test. Scale bar in a and b is equivalent to 10 μm .

morpholino directed against the translational start site—but not UTR—gives specific phenotype in the epidermis (see Supplementary Note and Supplementary Fig. 9 for details). The *lgl1* morphant displayed reduction in Lgl localization when anti-Lgl2 antibody was used suggesting that the antibody cross-reacts to Lgl1 in zebrafish. As published before, the *pen/lgl2* mutants do not exhibit appreciable staining for Lgl2 at 5 days post fertilization when anti-Lgl2 antibody was used²⁴. In absence of any detectable phenotype, we used this antibody to screen for *lgl2* mutants at 48 hpf. Despite the large variations in microridge lengths, the decrease in Lgl1 levels or absence of Lgl2 resulted in subtle but significant shift towards increase in shorter ridges as revealed by the bean plot and the decrease in medians (Fig. 3a,b). Consistently, the frequency distribution analysis revealed an increase in short (0–5 μ) ridges and reduction in the ridges that are longer than 100 μ (Fig. 3c). In addition, estimation of mean and variance for individual cells, followed by analysis of their distribution was done. We reasoned that the mean ridge length for a cell would decrease if there is a decrease in the number of longer ridges and increase in shorter ones. On the contrary, the mean ridge length for a cell would increase with increase in the number of longer ridges and decrease in shorter ridges. Similarly, the variance for each cell would either decrease or increase if the range of ridge lengths—from short to long ridges—gets smaller or larger, respectively. To maintain the robustness in the ridge length analysis in all subsequent experiments involving various genetic conditions, we followed these multiple ways of data analysis to assess the effects on ridges. The means and variances show significant decrease in Lgl1 and Lgl2 deficient cells (Fig. 3d). This analysis further suggested a decrease in the ridge lengths in absence of Lgl1/Lgl2 function. Interestingly, combined loss of both *lgl1* and *pen/lgl2* function did not result in further decrease in the length of microridges in most of the embryos (Fig. 3a–d).

Consistent with the decrease in ridge length in Lgl deficient embryos, live time-lapse imaging of microridges revealed that in contrast to wild-type, ridges fail to fuse and continue to remain shorter in the *lgl1* morphant peridermal cells during 23–30 hpf (Fig. 4a; Supplementary Videos 13–16). Reduction in Lgl2 levels also resulted in decreased F-actin levels at the basolateral domain (Fig. 4b) indicating Lgl's role in mediating F-actin assembly at the basolateral domain. There was no effect on formation or localization of tight junctions and adherens junctions in epidermal cells, which had reduced Lgl1 levels (Supplementary Fig. 2c). To test whether Lgl function is sufficient to increase microridge length in wild-type embryos, we increased Lgl levels by overexpression of *Xenopus lgl2* (Fig. 4c). Clonal analysis followed by quantification and analyses of ridge length distribution revealed that as compared with the surrounding peridermal cells, Lgl2 overexpression results in significant shift in length distribution towards longer, contiguous microridges similar to the *has/apkc* mutant (Fig. 4c,e–g). In addition, increase in Lgl leads to increased F-actin at the basolateral domain (Fig. 4d). Lgl2 overexpression did not have any overt cell adhesion or polarity phenotype as assessed by aPKC and E-cadherin staining (Supplementary Fig. 2d).

Microridge elongation in *has/apkc* depends on Lgl levels. We hypothesized that in the absence of aPKC function, increased Lgl levels at the apical domain cause microridges to become longer. To test the hypothesis, we reduced Lgl levels—using *penner/lgl2* mutant or knockdown of *lgl1*—in aPKC-deficient embryos. The bean plots, frequency distributions and distribution of means as well as variances clearly revealed a shift in the length distribution towards shorter ridges, suggesting rescue of the aPKC phenotype

(Fig. 5a–f; Supplementary Fig. 3a,b). These data suggest that in *has/apkc* mutants, microridge elongation occurs in an Lgl-dependent manner. To further confirm that the apically localized Lgl promotes an increase in the microridge length, we clonally expressed enhanced green fluorescent protein (eGFP)-Ezrin tagged mouse Lgl1 (mLgl1) in the peridermal cells. Ezrin is an essential component of the apical actin-based projections⁴⁴ and localizes to the microridges (Supplementary Fig. 1d). The eGFP-Ezrin-mLgl1 gets targeted to the apical domain and results in an increase in the ridge length as compared with the surrounding cells that do not express this fusion construct. The overexpression of eGFP-Ezrin does not lead to increase in microridge length. Similar to eGFP-Ezrin-Lgl1, overexpression of eGFP-mLgl1 also results in longer ridges in comparison to the neighbouring cells (Fig. 6; Supplementary Fig. 3c–f).

These lines of evidence indicate that Lgl1/2 promotes formation of long ridges presumably by increasing the fusion of shorter ridges. Furthermore, Lgl has the ability to regulate F-actin formation throughout the cortex but aPKC controls Lgl levels at the apical domain to restrict microridge length.

NMII activity is required for microridge elongation. Lgl was originally identified as a cytoskeletal protein, which forms a complex with NMII and gets released from the complex on activation by aPKC kinase activity^{28,29,31}. NMII is a motor protein having actin cross-linking and contractile properties⁴⁵. It is a major component of stabilized actin structures like stress fibres^{45,46}. The clonal expression of NMII heavy chain or light chain in peridermal cells revealed that both the chains localize to the microridges (Supplementary Fig. 4a). Despite the fact that both the chains would be overexpressed under CMV promoter, the clones did not exhibit any noticeable increase in the microridge length (Supplementary Fig. 4a). The quantification followed by distribution analysis revealed that while medians exhibit slight but significant shift on the higher side, neither frequency distribution nor analysis of means and variances revealed any significant increase in the microridge length suggesting negligible effect of the overexpression (Supplementary Fig. 4b–d). Immunolocalization using phospho-myosinII (pNMII) antibody—which detects phosphorylation of the regulatory light chain of NMII at the serine 19 residue—revealed that pNMII co-localizes with F-actin at the microridges in both wild-type and *has/apkc* mutants at 48 hpf (Fig. 7a). Temporal analysis indicated that pNMII localizes to the microridges as early as 20–24 hpf in both wild-type and aPKC-deficient embryos (Supplementary Fig. 5a). There was a quantifiable increase in localization of pNMII to the apical domain in *has/apkc* mutants at 36 hpf (Supplementary Fig. 5a,b).

To determine whether NMII activity is required for formation and elongation of microridges, NMII function was inhibited using chemical inhibitor Blebbistatin, which suppresses MyosinII ATPase activity and actin–myosin cross-linking⁴⁷. Treatment of embryos with Blebbistatin for 1.5 h at a concentration of 10 μ M—low enough to keep the cortical actin and cellular architecture intact—resulted in increase in shorter ridges in wild-type embryos at 48 hpf. In *has/apkc* mutant, the treatment resulted in a shift in the length distribution towards shorter ridges as compared with the untreated mutants (Fig. 7b–e). Blebbistatin also inhibited elongation of microridges when the treatment was done at early stages while the microridges are growing by fusion—during 20–22 hpf in aPKC-deficient and between 27 and 30 hpf in wild-type embryos (Supplementary Fig. 5c,d). This analysis suggests that NMII function is required for elongation of ridges and maintenance of their length in wild-type as well as in aPKC-deficient embryos.

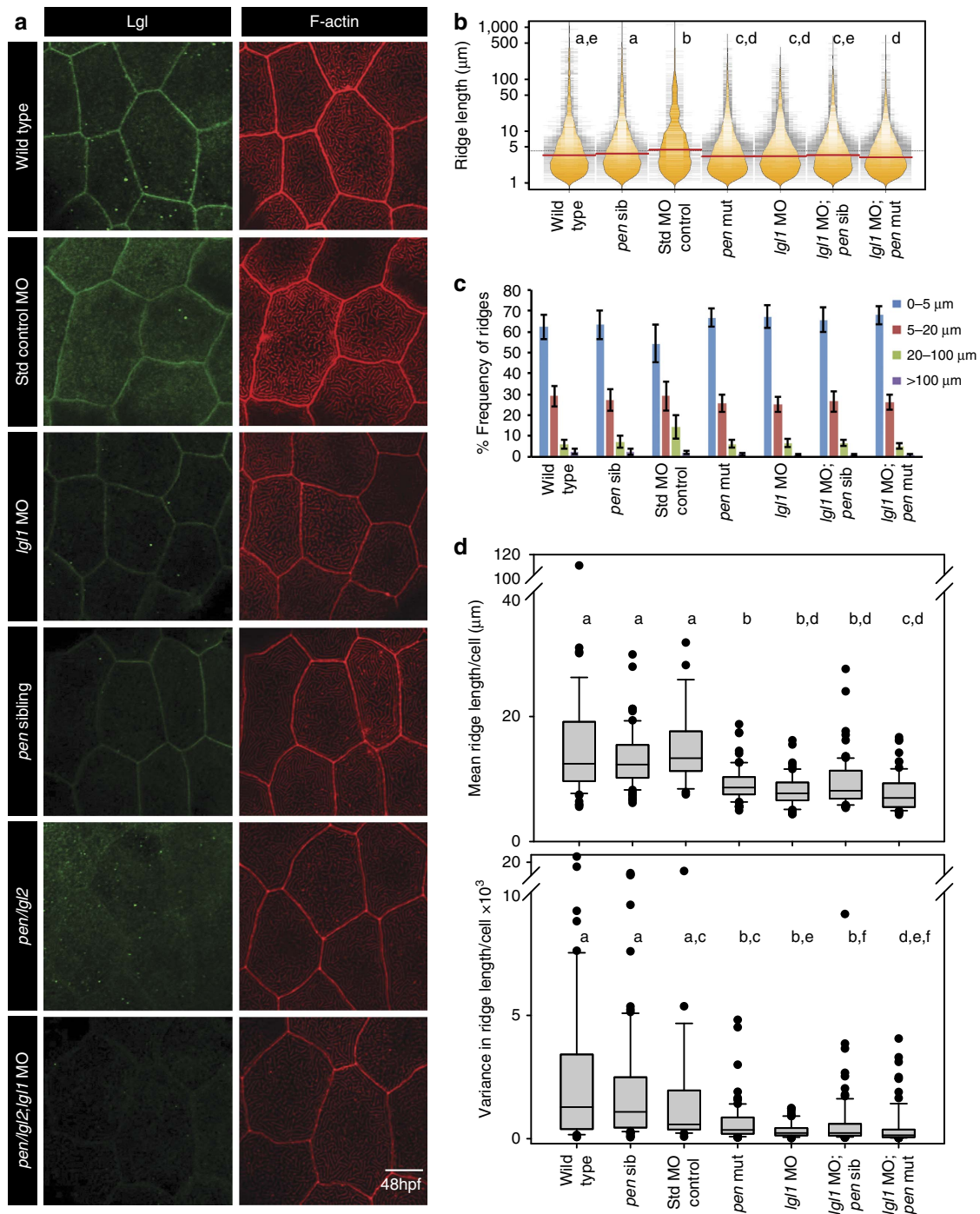


Figure 3 | Lgl functions in the elongation of microridges in the apical domain. Immunofluorescence images of Lgl and F-actin in the apical domain of peridermal cells in given genetic conditions or morpholino injections at 48 hpf (**a**). Visualization of the distribution of ridge lengths and medians at 48 hpf, in various genetic conditions mentioned, using violin plots and horizontal lines, respectively followed by estimation of percentage frequency distribution of ridges in short (0–5 μm), intermediate (5–20 μm), long (20–100 μm) and very long (>100 μm) categories (**b**) followed by estimation of percentage frequency distribution of ridges for individual cells and comparison of the distributions of the means and variances across various genotypes using box-whisker plots (**d**). In **b** and **d** the distributions denoted by same alphabet or distributions that share an alphabet in common (when denoted by multiple alphabets) do not differ significantly (Dunn's multiple comparisons test, P -value < 0.05; see Methods section for details). In **c** s.d. is shown by error bars. Scale bar in **a** is equivalent to 10 μm . MO, morphant/morpholino; Std, standard.

To check whether function of active NMII is sufficient to increase microridge length, we overexpressed the constitutively active form of myosin light chain kinase (MLCK-CA), which is a specific activator of NMII function. MLCK-CA messenger RNA (mRNA) injected embryos showed obvious increase in pNMII staining and phenocopied the *has/apkc* mutant phenotype at

48 hpf (Fig. 7f). We conclude that the phosphorylated or active form of NMII is necessary and sufficient to increase and maintain the microridge length.

Lgl and active NMII cooperate to regulate microridge length. Lgl genetically and physically interacts with NMII and regulates

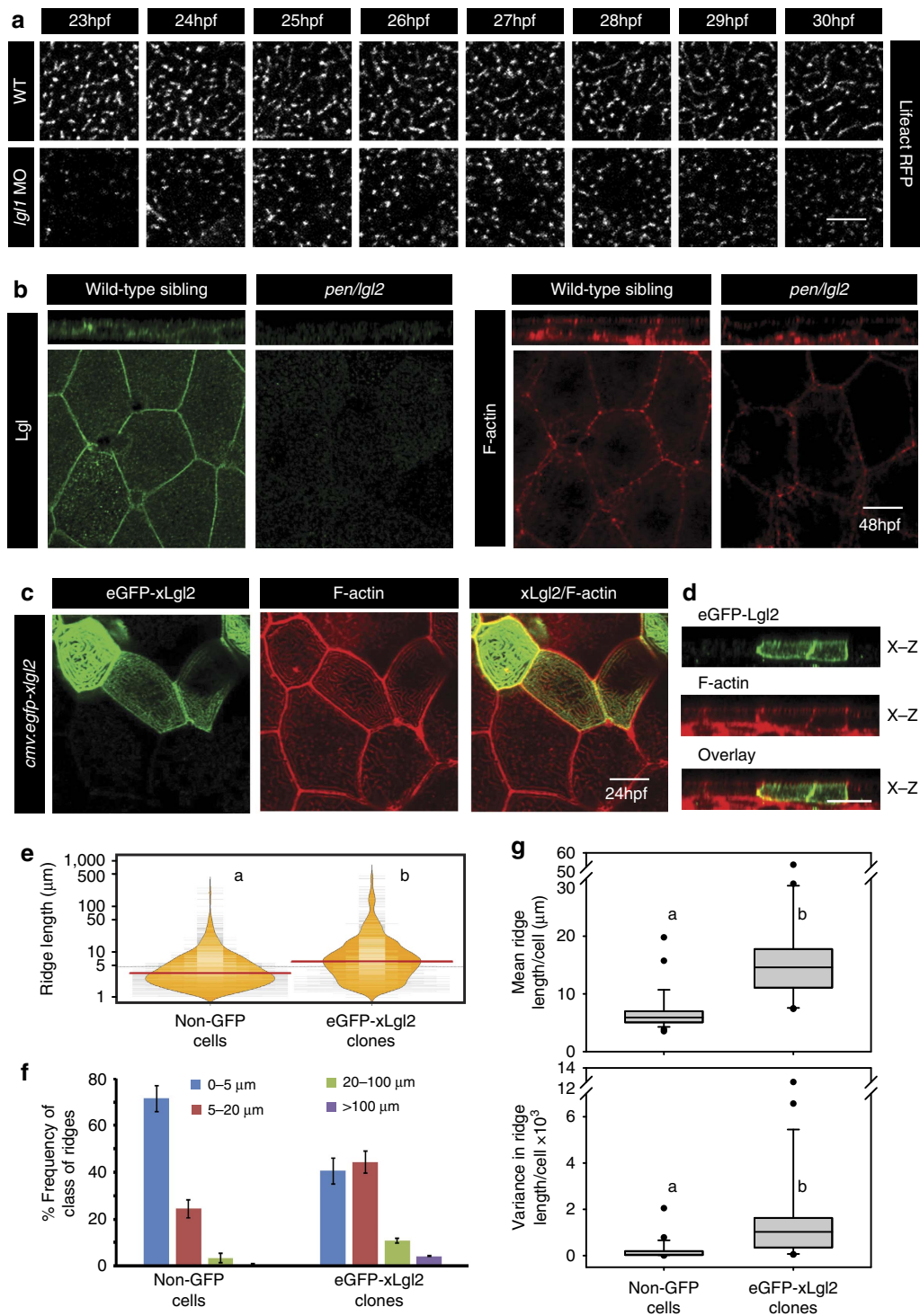


Figure 4 | Lgl regulates the length of microridges by promoting their fusion. Live time-lapse imaging of microridge elongation (**a**) in clones expressing lifeActRFP under CMV promoter in wild-type and *lgl1* morphant embryos during 23–30 hpf. Immunolocalization of Lgl and F-actin at the basolateral domain in wild-type and *pen/lgl2* mutant at 48 hpf (**b**). Confocal images of immunostaining using anti-GFP antibody and phalloidin in wild-type embryos-injected with eGFP-xLgl2 construct under CMV promoter at 24 hpf (**c**) and their orthogonal sections (**d**). Visualization of the distribution of the ridge lengths and medians in eGFP-xLgl2 expressing clones and surrounding non-GFP cells using bean plots (**e**). The frequency distribution of ridges in short (0–5 μm), intermediate (5–20 μm), long (20–100 μm) and very long (>100 μm) categories (**f**). The box-whisker plots (**g**) represent the distributions of means and variances per cell in eGFP-xLgl2 expressing clones and surrounding non-GFP cells. Data presented in **e–g** is based on ridge-length measurements done on phalloidin stainings performed in the eGFP-xLgl2 injected embryos at 24 hpf. In bean plots (**e**) and box-whisker plots (**g**) the alphabets ‘a’ and ‘b’ represent significant difference in median values at $P < 0.05$ (pairwise multiple comparison using Dunn’s Method). Error bars in **f** represent the s.d. Scale bars in **a–d** correspond to 10 μm .

its activity and distribution by binding to the coiled-coil rod domain of the heavy chain of NMII (refs 25,26,28–30,34,35). Immunostainings followed by analysis of colocalization

coefficients showed that Lgl and pNMII show increased colocalization at the microridges in *has/apkc* mutants as compared with wild type siblings at 48 hpf (Fig. 8a,b). To check

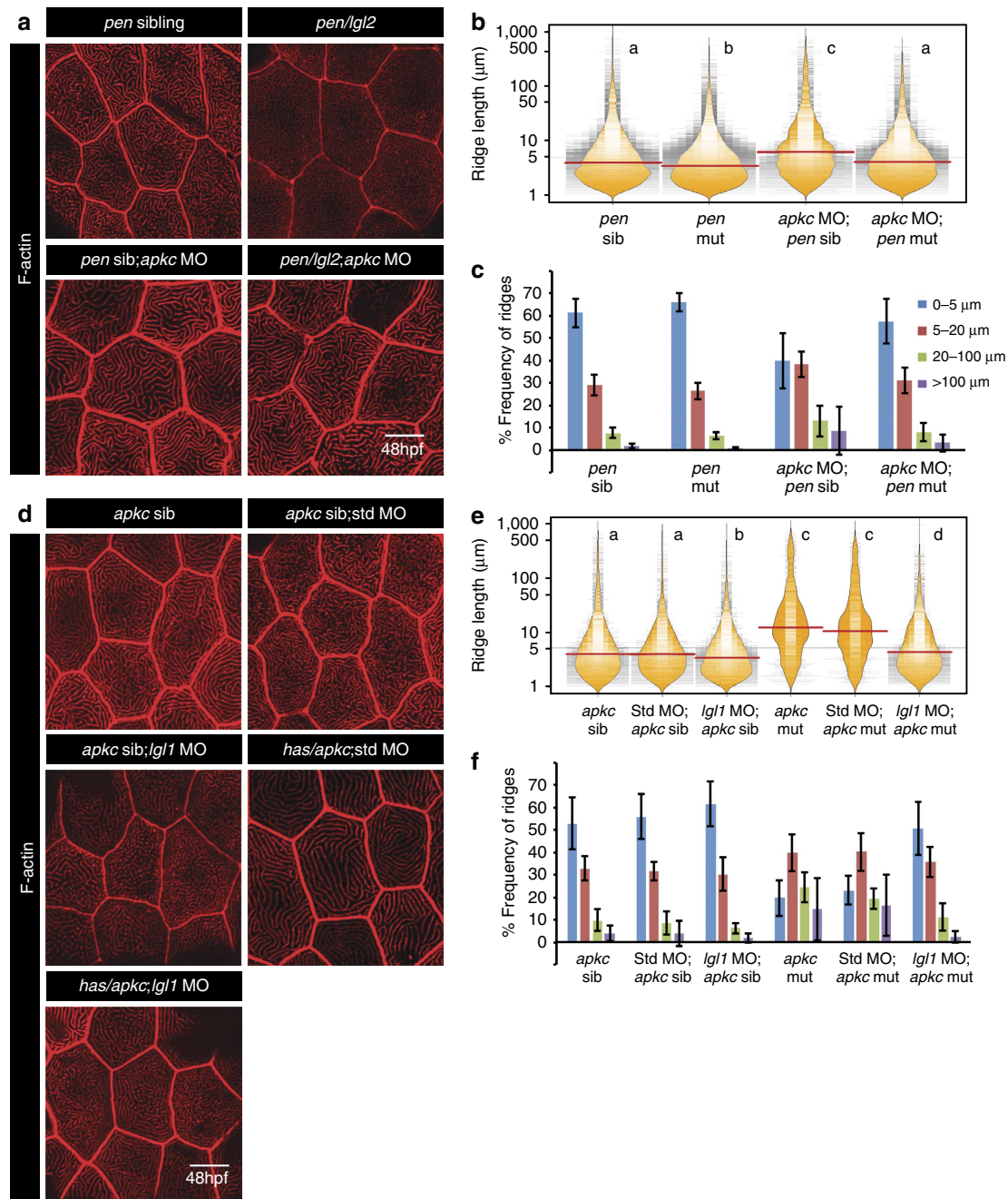


Figure 5 | Microridge elongation in aPKC-deficient embryos occurs in an Lgl-dependent manner. Phalloidin stainings (**a,d**) at 48 hpf in genotypes mentioned. Ridge length estimation followed by visualization of the spread and frequency of their lengths and medians using bean plots (**b,e**). The frequency distribution of ridges (**c,f**) in short (0–5 μm), intermediate (5–20 μm), long (20–100 μm) and very long (>100 μm) categories across the above mentioned genotypes. In **b** and **e** the distributions sharing the same alphabet do not differ significantly (Dunn's multiple comparisons test, P -value < 0.05). Error bars in **c** and **f** represent the s.d. Scale bars in **a** and **d** corresponds to 10 μm .

whether both Lgl and active NMII are essential to regulate microridge length, *lgl1* knockdown was achieved in embryos over-expressing MLCK-CA. Down regulation of *lgl1* in MLCK-CA overexpression background rescued the long microridge phenotype caused due to increased NMII activity (Fig. 8c–f). Similarly, overexpression of MLCK-CA did not yield longer microridge phenotype in *pen/lgl2* mutant (Supplementary Fig. 6a–d). Furthermore, Lgl2 overexpression resulted in mild increase in pNMII levels (Supplementary Fig. 7a). Consistently, inhibition of NMII activity by Blebbistatin in Lgl2 over-expressing peridermal cells resulted in smaller microridges at 24

and 30 hpf (Supplementary Fig. 7b,c). We conclude that both Lgl and active NMII cooperate in zebrafish peridermal cells to regulate microridge length.

F-actin polymerization in microridge elongation and maintenance. We further investigated the contribution of F-actin polymerization in the elongation and maintenance of ridges under various genetic conditions. Microridges are formed of F-actin filaments organized perpendicular to the plasma membrane¹, similar to other actin-based projections⁴⁸.

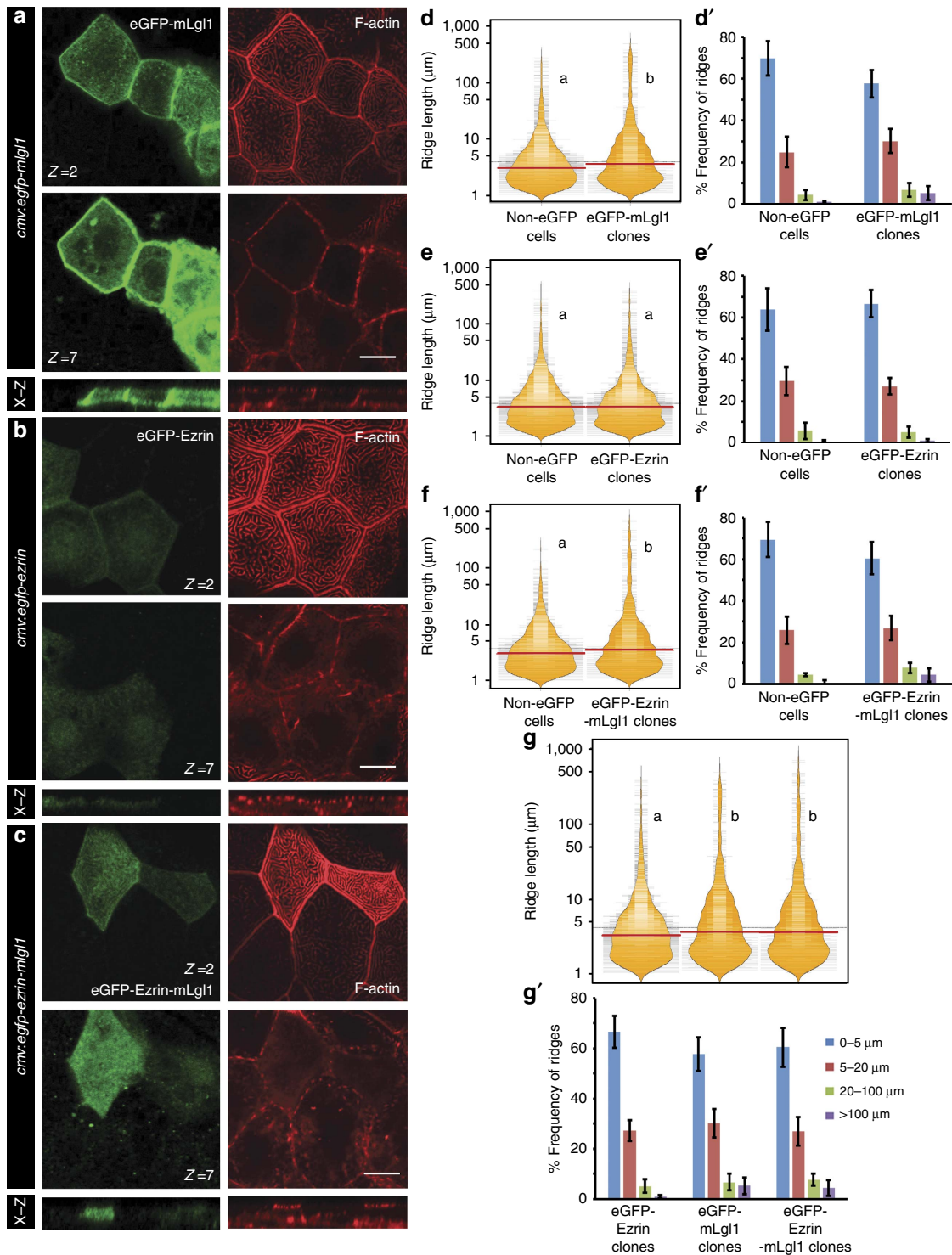


Figure 6 | Apically localized Lgl promotes an increase in the microridge length. Confocal sections at the apical ($z = 2$) and basolateral level ($z = 7$) of the peridermal cells stained (a–c) for GFP and F-actin at 30 hpf in wild-type embryos injected with eGFP-mLgl1 (a) eGFP-Ezrin (b) and eGFP-Ezrin-mLgl1 (c) under CMV promoter along with their corresponding orthogonal sections. Visualization of the distribution of ridge lengths and medians—estimated from clones expressing eGFP-mLgl1 (d) eGFP-Ezrin (e) and eGFP-Ezrin-mLgl1 (f) and their corresponding non-GFP controls using bean plots. Comparison between the ridge lengths exhibited by clones expressing eGFP-Ezrin, eGFP-mLgl1 and eGFP-Ezrin-mLgl1 (g). The frequency distribution of ridges in short (0–5 μm), intermediate (5–20 μm), long (20–100 μm) and very long (>100 μm) categories for clones expressing eGFP-mLgl1 (d’), eGFP-Ezrin (e’) and eGFP-Ezrin-mLgl1 (f’) along with their corresponding non-GFP controls. The comparison between frequency distributions observed in clones expressing eGFP-Ezrin, eGFP-mLgl1 and eGFP-Ezrin-mLgl1 (g’). Quantifications in (d–g) and (d’–g’) are based on phalloidin stainings performed at 30 hpf in the embryos injected with the above mentioned eGFP constructs. Note the minimal localization of eGFP-Ezrin-mLgl1 and eGFP-Ezrin to the basolateral cortex as compared with eGFP-mLgl1. The distributions represented by two different alphabets in d–g show significant difference at $P < 0.05$ (Dunn’s multiple comparisons test). Error bars in (d’–g’) represent the s.d. Scale bars in a–c correspond to 10 μm .

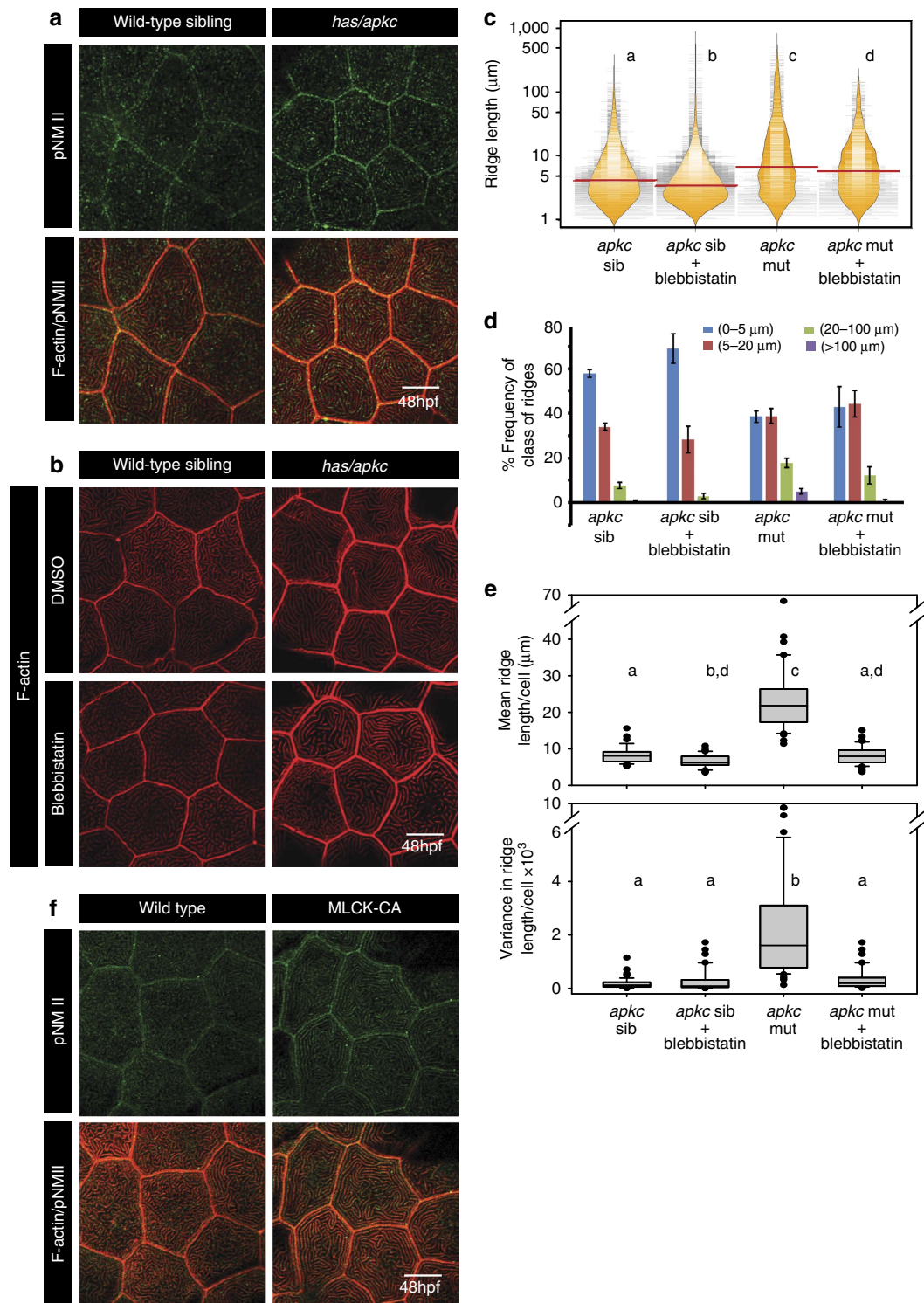


Figure 7 | Activity of non-muscle myosinII (NMII) is essential and sufficient for elongation of microridges. Immuno-colocalization using anti pNMII antibody and phalloidin in wild-type and *has/apkc* mutant at 48 hpf (**a**). Wild-type and *has/apkc* mutant treated with 10 μ M Blebbistatin at 48 hpf and stained using phalloidin to visualize F-actin (**b**). Graphical representation of the distribution of ridge lengths and medians of Blebbistatin treated and control embryos at 48 hpf using bean plots (**c**). The same data is presented as percentage frequency distribution of ridges in short (0–5 μ m), intermediate (5–20 μ m), long (20–100 μ m) and very long (>100 μ m) categories (**d**). Distribution of means and variances of ridge lengths (**e**) for individual peridermal cells- in wild-type sibling and *has/apkc* mutant treated with DMSO and Blebbistatin at 48 hpf—presented in box-whisker plots. Immuno-colocalization using anti pNMII antibody and phalloidin staining in wild-type embryos and embryos over-expressing constitutively active MLCK at 48 hpf (**f**). In **c** and **e** the distributions sharing the same alphabet do not differ significantly (Dunn’s multiple comparisons test, P -value < 0.05). In ((**e**) top) the distributions for *apkc* sib and *apkc* sib + Blebbistatin are considered statistically significantly different at $P = 0.058$. Error bars in **d** are for the s.d. Scale bars in **a**, **b** and **f** are equivalent to 10 μ m.

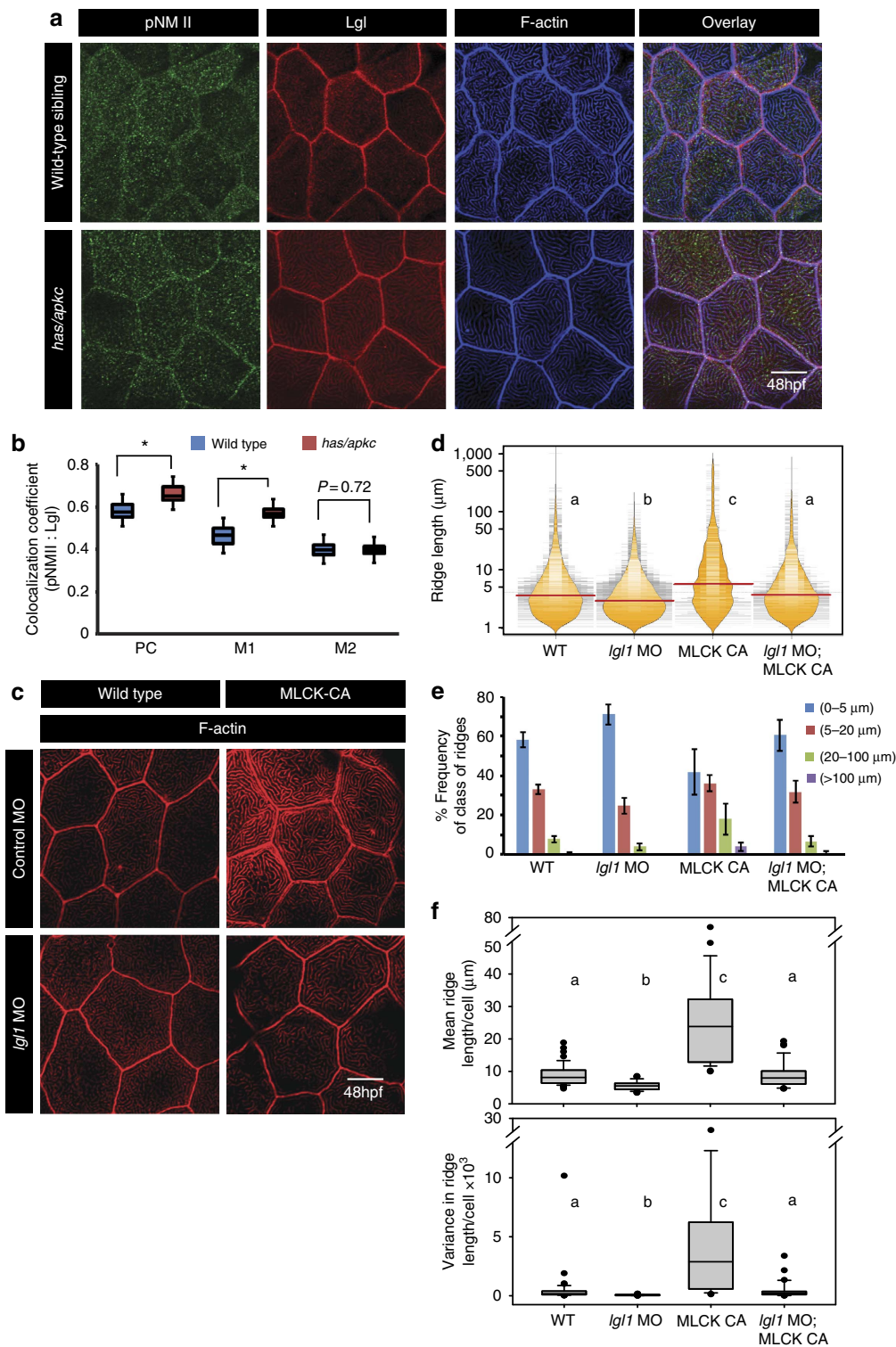


Figure 8 | Both *Lgl* and active MyosinII are required to build long ridges. Immunocolocalization using anti pNMII, anti-Lgl2 antibodies and phalloidin (**a**) in wild-type and *has/apkc* mutant at 48 hpf. Graphical representation (**b**) of colocalization coefficients for pNMII and Lgl by Pearson's method and Manders' overlap of pNMII with Lgl (M1) and Lgl with pNMII (M2) in wild-type and *has/apkc* mutant embryos at 48 hpf. Phalloidin stainings (**c**) in embryos injected with control morpholino, MLCK-CA + control morpholino, *lgl1* morpholino and MLCK-CA + *lgl1* morpholino at 48 hpf, followed by ridge length measurements and visualization of distribution of ridge lengths and medians using bean plots (**d**). The same data is presented as percentage frequency distribution of ridges in short (0–5 μm), intermediate (5–20 μm), long (20–100 μm) and very long (>100 μm) categories (**e**). The box-whisker plots (**f**) represent distributions of means and variances of ridge lengths for individual cells from various genetic conditions. In **d** and **f**, the distributions sharing the same alphabet do not differ significantly (Dunn's multiple comparisons test, P -value < 0.05). Error bars in **e** are for the s.d. Asterisks in **b** indicate significant difference at $P < 0.001$ by Student's *t*-test. Scale bars in **a** and **c** is equivalent to 10 μm.

We treated *has/apkc* mutants, MLCK-CA embryos and wild-type embryos at 48 hpf with Latrunculin A. In addition, we also treated 5-day-old larvae with Latrunculin because the microridges are long and convoluted in 5-day-old larvae, similar to 2-day-old *has/apkc* mutants. Latrunculin associates with actin monomers and prevents them from getting incorporated into filaments⁴⁹. Thus, Latrunculin treatment would lead to net increase in actin depolymerization. Treatment of 48 hpf wild-type and *has/apkc* sibling embryos with a brief pulse of Latrunculin resulted in shortening of microridges. After treatment, the occurrence of short ridges increases significantly in wild-type and *has/apkc* sibling at 48 hpf, as revealed by the bean plot, frequency distribution and analysis of means and variances. These data suggest that actin polymerization is required to maintain the length of these structures. Surprisingly, microridges in *has/apkc* mutants and MLCK-CA over-expressing peridermal cells remained relatively unaffected by Latrunculin treatment at 48 hpf (Fig. 9a–h). However, both *apkc* morphants and MLCK-CA over-expressing embryos were susceptible to Latrunculin treatment when the ridges are actively growing in these two conditions, leading to shorter ridges (Supplementary Fig. 8a). Similarly, in 5-day-old wild-type larvae and in Lgl2 overexpression condition, Latrunculin treatment resulted in decrease in the length of microridges (Supplementary Fig. 8b).

These data suggest that actin polymerization is required for ridge elongation at early developmental stages. In *has/apkc* mutant and MLCK-CA overexpression condition actin filaments are stable and are less dependent on actin polymerization for their maintenance. In Lgl2 overexpression condition and in 5-day-old wild-type larvae, microridges continue to depend on actin polymerization to maintain their length.

Discussion

Whether cell polarity regulators control the formation of apical projections has remained poorly understood. Here we have used microridges in the head peridermal cells as a paradigm to show that the two key polarity regulators, aPKC and Lgl1/Lgl2 regulate formation of these actin-based apical projections.

In brush border or microvilli of the enterocytes, it has been shown that Lkb1/Par4 links cell polarity with brush border formation through a small G protein Rap2A (ref. 50). A recent report shows that knockout of *Crb3*—a vertebrate paralogue of *Drosophila* cell polarity gene *crumbs*—results in disorganized and shorter microvilli in mouse enterocytes⁵¹. Our analysis presented here show that aPKC and Lgl1/Lgl2 antagonistically control the elongation of microridges, which are laterally long actin projections. We show that functions of Lgl1/Lgl2, pNMII and the process of actin polymerization are important for building microridges in the peridermal cells. We propose that low levels of Lgl and pNMII at the apical cortex promote the fusion of short ridges to gradually build long ridges. In addition, pNMII and actin polymerization are important for ridge elongation as well as in the maintenance of longer ridges in the wild type. The function of aPKC is essential to control the levels of Lgl and pNMII at the apical cortex. In the absence of aPKC function, increased levels of pNMII and Lgl lead to actin polymerization-dependent precocious elongation of ridges. Thus, we have identified a hitherto unknown function for Lgl—a regulator of basolateral domain—at the apical cortex in zebrafish epidermal cells. We have also unravelled the functional significance of removal of Lgl from the apical domain by aPKC, a mechanism that is conserved in a variety of epithelial systems across various phyla^{8,40,41}. We have been able to uncover these later and subtler functional aspects of cell polarity regulators without having profound effect on cell polarization possibly due to presence of maternal contribution of

Lgl and aPKC (refs 22,36) and functional redundancy between aPKC paralogues in zebrafish⁵².

Previous report indicates that *pen/lgl2* transcripts are contributed maternally and that zygotic expression is observed in the basal epidermis at 24 hpf (ref. 22). Our recent analysis by *in situ* hybridization shows that both *lgl1* and *lgl2* are expressed ubiquitously during epiboly stages (ReR, ID and MS, unpublished observations). Thus, Lgl1/Lgl2 might be inherited by the periderm from its precursor, the enveloping layer, and their levels are subsequently maintained by basal level expression of both the paralogues. It is intriguing that the loss-of-function of *lgl* paralogues results in such subtle phenotypes in the zebrafish epidermis at early stages. The knockdown of *lgl1*, loss-of-function of *lgl2* and the combined loss of *lgl1/lgl2* function yield quantitative reduction in the length of microridges. On the other hand, overexpression of Lgl1/Lgl2 as well as apically targeted Lgl1 results in robust increase in the ridge lengths. Thus, while Lgl function is sufficient to increase the ridge length and is necessary for their elongation to build long ridges, it might not be essential for their formation. Furthermore, though Lgl overexpression results in formation of longer ridges, it only partially recapitulates the aPKC phenotype in quantitative terms indicating that aPKC governs multiple pro-elongation factors during ridge formation. It appears that the function of ridges are of vital importance and therefore their formation is redundantly regulated by other polarity components besides Lgl. Such redundant mechanisms have been reported for maintenance of cell polarity in *Drosophila* epithelial tissues^{53–56}. Thus, further investigations are required to identify additional components or polarity regulator/s that act in conjunction with the two Lgls in formation of apical microridges.

Recently, zebrafish peridermal microridges have been characterized with respect to their composition and dynamics. It has been shown that actin regulators cortactin and VASP localize to the ridges. Besides, actin polymerization and activities of Arp2/3 and PI3K signalling have been shown to be important for the maintenance of microridge length⁵⁷. Similar to this earlier report⁵⁷, our analysis suggests that actin polymerization is essential for the formation of actin microridges. However, in contrast to their finding⁵⁷, we have consistently found that Blebbistatin treatment results in shortening of the ridges suggesting that pNMII has an essential role in microridge formation. Interestingly, in contrast to wild type, once formed, the longer ridges in *has/apkc* mutants become relatively stable and hence do not rely on actin polymerization for their maintenance. However, such stable structures might be detrimental for a growing epithelial system like epidermis, which would require plasticity. Hence a slower mechanism of building ridges by controlling levels of active form of myosinII and maintaining persistently low levels of Lgl must have evolved to form plastic microridges.

Microridges are present on several squamous epithelial cells. However, the regulation of their formation has remained unclear due to lack of a suitable model. This study establishes the possibility of using zebrafish epidermis as a model to unravel the molecular mechanisms involved in the formation of ridges. It is intriguing to see large variations in the patterns as well as lengths of the microridges in head peridermal cells within an embryo as well as across various embryos from the same parents or different parents while the embryos develop. These variations do not easily reveal the changes in lengths by qualitative assessment. Even after quantification, the variations and non-normal distribution of the data demand robust analysis by non-parametric statistical tests to assess the effect. Here we have employed methods consisting of (a) a new data visualization method using bean plots, (b) frequency distribution of ridge

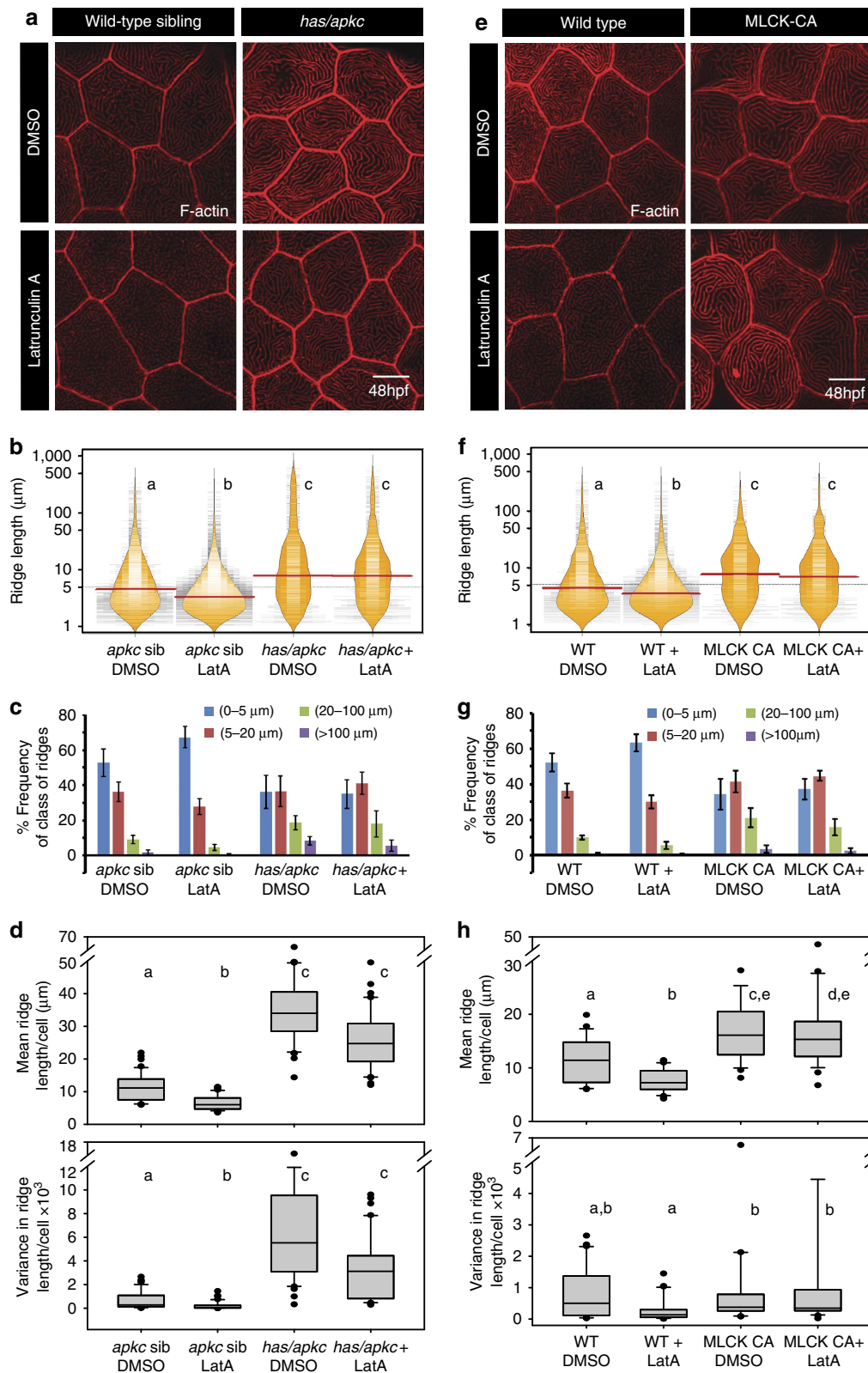


Figure 9 | The loss of aPKC function and overexpression of MLCK-CA results in formation of Latrunculin resistant stable microridges. Phalloidin stainings of *has/apkc* sibling and mutant embryos (a) and wild type and MLCK-CA overexpression embryos (e) treated with Latrunculin A. Visualization of the spread and frequency of ridge lengths and medians from the given genotypes and treatments using bean plots (b,f). Estimation of percentage frequency distribution of ridges in short (0–5 μm), intermediate (5–20 μm), long (20–100 μm) and very long (>100 μm) categories (c,g). Estimation of cell wise means and variances of ridge lengths based on phalloidin stainings (d,h). In b,d,f and h, the distributions sharing the same alphabet do not differ significantly (Dunn’s multiple comparisons test, P -value < 0.05). The two distributions in ((h) top), WT DMSO and MLCK-CA + LatA, are different at $P = 0.061$. Error bars in c and g are for the s.d. Scale bars in a and e are equivalent to 10 μm .

lengths in various bins, (c) analysis of means and variances for individual cells and analysis of their distribution, (d) statistical analysis using non-parametric tests such as Kruskal–Wallis test and Dunn's pairwise comparison. This methodology has allowed reliable detection of subtle differences amongst the genotypes.

To summarize, we have identified a novel regulation of microridge formation by antagonistic interactions between aPKC and Lgl. Importantly, we have identified the significance of Lgl removal from the apical domain by aPKC in vertebrate epithelial cells. Our analyses presented here suggest that formation of apical projections is under the control of mechanisms involved in establishment and maintenance of epithelial cell polarity.

Methods

Ethics statement. For zebrafish maintenance and experimentation, guidelines recommended by the Committee for the Purpose of Control and Supervision of Experiments on Animals (CPCSEA), Govt. of India, were followed.

Fish strains. For experiments in wild-type embryos, the Tübingen (Tü) strain was used. Alleles *has^{m567}* and *pen¹⁰⁶* were used for the mutant studies presented here^{22,36}. Tg(cldnB:lynEGFP) line was used to visualize plasma membrane wherever necessary³⁷.

Whole-mount immunostaining. Whole-mount immunostainings in zebrafish embryos were performed as before²³. For most of the stainings, embryos were fixed overnight in 4% PFA followed by permeabilization in methanol at -20°C for at least overnight. For pNMII, and GFP staining, embryos were processed for staining immediately after overnight fixation in PFA. For Lgl stainings done along with phalloidin, only PFA fixation was used. For co-staining of Lgl and other markers, the overnight PFA fixed samples were post-fixed in methanol. Though there are differences in Lgl staining intensities at the apical domain in the absence and presence of methanol post-fixation, we consistently observed increased apical Lgl in *has/apkc* mutant and *apkc* morphants as compared with siblings. Notably, in *has/apkc* mutant periderm apical Lgl staining is enhanced but the siblings show near absence of the apical Lgl staining after methanol post-fixation. For staining using anti-ZO-1 antibody (1:100; ZYMED Labs, Invitrogen; 61–7,300), embryos were fixed in Dent's fixative (80:20 methanol: DMSO) overnight at -20°C . Fixed or post-fixed embryos were washed 5 times with PBT (PBS + 0.8% Triton-X 100) and incubated in 10% normal goat serum (NGS) in PBT for 3 h at room temperature. The embryos were incubated overnight with primary antibodies, diluted appropriately in 1% NGS in PBT, at 4°C . Antibodies and their dilutions: anti-Lgl2 (1:400)²³, monoclonal anti-E-cadherin (1:100; BD Transduction Labs; 610,182), anti-GFP (1:200; Torrey Pines Biolabs; TP401), monoclonal anti-GFP (1:40; Genei, Bangalore), anti-aPKC (1:750; Santa Cruz Biotechnology; sc-216), anti-pMyosinII (1:25; Cell Signaling Technologies; 3,671; 3675), and anti-Ezrin (1:250; Santa Cruz Biotechnology; sc-32759). Embryos were then washed five times in PBT and incubated in secondary antibodies, appropriately diluted in 1% NGS in PBT, for 4 h at room temperature. Secondary antibodies conjugated with Alexa 488 (1:250; Molecular Probes; A-11034, A-11029), Alexa 546 (1:250; Molecular probes; A-10036), Alexa 568 (1:250; Molecular probes; A11011) or Alexa 647 (1:250; Molecular Probes; A-21236, A-21245), Cy3 (Jackson ImmunoResearch Labs; 115-165-144, 115-165-146) or Cy5 (1:750) (Jackson ImmunoResearch Labs; 115-175-144, 115-175-146) were used. Subsequently, embryos were washed 5 times in PBT, post-fixed in 4% PFA and upgraded in glycerol for imaging using confocal microscopy. All samples required to be stained using either Alexa 488 (1:40; Molecular Probes; A12379), Rhodamine (1:40; Molecular Probes; R415) or Alexa 647 conjugated phalloidin (1:40; Molecular Probes; A22287) were fixed overnight in 4% PFA in PBS at 4°C .

Drug treatment. Blebbistatin (B0560, Sigma) and Latrunculin A (L5163, Sigma) were dissolved in DMSO at a stock concentration of 100 mM and 1 mM, respectively. Working dilutions of Blebbistatin and Latrunculin A, at final concentrations of 10 and 2 μM , respectively, were prepared in E3 buffer containing 1% DMSO. Embryos were treated with Blebbistatin for 1.5 h and with Latrunculin A for 30 min at 29°C , while control embryos were incubated in 1% DMSO for the same time periods. Embryos were fixed at the appropriate stages and processed further for immunostainings.

Morpholino, mRNA and plasmid injections. Antisense morpholino oligonucleotides (Gene Tools, LLC), were microinjected in the 1–2 cell stage embryos at the following concentrations: *lgl1*-MO^{*lgl1-atg*} 5'-CCGTCTGAACCTAACTTCA TCATC-3' (250 μM) (refs 42,43), *lgl1*-MO^{*lgl1-utr*} 5'-TGAAGCCGAATCAGAG GTAATCAC-3' (300 μM) (refs 42,43), *aPKC λ* -MO aPKC λ -atg 5'-TGTCCCGCA GCGTGGCATTATGGA-3' (100 μM) (ref. 36). Standard control morpholino 5'-CCTCTTACCTCAGTTACAAATTTATA-3' or 5 base mismatch control morpholino 5'-CCCTCTCAACGTAAGTTCATGATC-3' (Gene Tools, LLC) was

also used as a control for *lgl1* morpholinos. MLCK-CA construct⁵⁸ was modified to remove (*nos1*-3'UTR) and capped mRNA was transcribed using the T7 mMessage mMachine kit (Ambion; AM1344). The mRNA was injected at a concentration of 300 ng μl^{-1} in the 1–2 cell stage embryos. Xenopus GFP-Lgl2 construct⁵⁷, pCMV LifeAct-TagRFP plasmid (ibidi; 60,102), mouse GFP-Lgl1 (ref. 33) were injected at a concentration of 100 ng μl^{-1} . Zebrafish Ezrin cDNA (BC139506.1) was cloned into the pCRII-TOPO vector (Invitrogen; K460001) and subcloned into the eGFP-Lgl1 vector using EcoRI (NEB; R0101S, R3101) restriction sites to make the eGFP-Ezrin-Lgl1 fusion construct. The control eGFP-Ezrin construct was made by restriction digestion using BamHI (NEB; R0136S) to release mLgl1 from the eGFP-Ezrin-Lgl1 fusion construct. The CMV-GFP-NMHC II-A plasmid used to overexpress the heavy chain of non-muscle myosin-IIA was a gift from Robert Adelstein (Addgene plasmid #11347) (ref. 59), whereas the Myl12.1-eGFP construct⁶⁰ was a gift from C. P. Heisenberg. All constructs were injected at a concentration of 100 ng μl^{-1} .

Microscopy and image analysis. Confocal imaging was done in the head (dorsal) epidermis on the Zeiss LSM 510 Meta confocal microscope having an EC Plan-Neofluar $\times 40/1.30$ oil-immersion objective lens or on Zeiss LSM 710 having Plan-Apochromat $\times 40/1.3$ oil-immersion objective with an optical $2 \times$ zoom. Image size was 1,024 \times 1,024 with an averaging of 4. The pinhole values were kept as 1 Airy Unit. For time-lapse live imaging, embryos injected with pCMVLifeAct-TagRFP plasmid were dechorionated and screened for epidermal clones. Post screening, embryos were anaesthetized with 0.04% MESAB (Sigma; A5040) and mounted in 0.2% low melting agarose in plastic dishes with cover slip bottoms. Imaging was done on Zeiss LSM 5 Exciter equipped with temperature-controlled chamber using Plan-Apochromat $\times 63/1.40$ oil objective lens with an optical $\times 1.5$ zoom. Image size was 512 \times 512 with an averaging of 4. The pinhole value for 543 laser line was kept at 106 μm and confocal stacks were captured at a slice interval of 0.411 μm . The capture rate was one frame per 12 min and played at a rate of 6 frames per second for Supplementary Videos 1–8, 13–16. Zeiss LSM 710 was used for capturing movies with higher temporal resolution using acquisition speed of two frames per minute and played at a rate of 6 frames per second for Supplementary Videos 9–12. The Image5D plug-in from ImageJ was used for image processing and analysis of live movies.

Imaging conditions were kept uniform across most of the experiments. Occasionally, PMT gains were slightly re-calibrated to uniformly suit imaging of all the genotypes in a given set. This helps avoid saturation of a stronger signal in a particular genotype and at the same time allows detection of a weaker signal in some other genotype. For colocalization measurements involving marker pairs aPKC:F-actin, Lgl:F-actin, pNMII:F-actin and pNMII:Lgl, imaging conditions were kept same across all the genetic conditions.

To improve visualization in figure panels, some of the images were digitally processed using Adobe Photoshop CS6. However, all the quantifications have been done on raw unprocessed images.

Estimation of microridge perimeter and surface area quantification. Embryos stained with Rhodamine phalloidin were used for quantification using ImageJ. To calculate microridge perimeter and number, the cell outline was traced in the confocal apical slice displaying microridges. Images were smoothed and thresholded such that the outlines of the ridges were clearly defined. The Analyze Particle command was used to detect the number and perimeter of the edges of microridges. Images were thresholded for a second time, if required, to detect the edge of microridges that could not be marked clearly in the first round. The Magic Wand tracing tool was used for manual detection and selection of microridges after second round of thresholding.

For each genetic condition, the perimeter quantification of microridges was done on 4–8 cells per embryo. Multiple embryos from various experimental sets were used to obtain the data. The details of the number of ridges, cells, embryos and experimental sets are provided as an excel sheet (Supplementary Data 1).

To estimate the surface area of the plasma membrane, *has/apkc* mutants in the background of Tg(cldnB:lynEGFP) line were stained with anti-GFP antibody. As published earlier⁶¹, to calculate the surface area, cell outlines were marked in each confocal section using the Measure Stack plug-in of ImageJ. Basolateral surface area was estimated by multiplying the perimeter of each slice by the slice thickness and adding it to the area of the first and the last slice. Area occupied by microridges in membrane folds was quantified by first obtaining the perimeter of microridges as mentioned earlier. This perimeter multiplied by the section thickness and summing this for all the confocal slices encompassing the ridges yields the membrane area for the ridges. The total surface area was estimated by adding up the basolateral surface area and the area occupied by microridges.

For surface area quantification, five cells from each embryo and a total of six embryos ($N = 6$; $n = 30$) were quantified for each genetic condition.

Colocalization measurements. Localization of proteins to microridges was detected and quantified using the JACoP plugin in ImageJ. Boundaries of individual cells were marked at the apical slice displaying microridges. Five cells from each embryo and a total of eight embryos from two different experiments were used for analysis ($N = 8$, $n = 40$). Images were thresholded manually to mark

microridges and the Pearson correlation coefficient and Manders' overlap coefficient were calculated. Manders' coefficient M1 indicates fraction of A overlapping B, while M2 indicates fraction of B overlapping A.

Statistical analysis. Bean plots were used to visualize distribution of microridge perimeters across different genotypes. Microridge perimeter data for each genotype was collated and Bean plots along with medians were plotted in R statistical software. In addition, mean ridge length and variance was estimated for individual cells from every genotype/treatment. The distribution of the means and variances for cells from each genotype were represented using Box-whisker plots. The data analysis was done using Kruskal–Wallis one-way analysis of variance on ranks followed by pairwise multiple comparison procedures using Dunn's Method. The statistical significance of pairwise comparisons is denoted using alphabet(s) associated with each distribution in the graphs. The two distributions are not significantly different at $P < 0.05$ when they are denoted by the same alphabet or when they share one alphabet in common when denoted by multiple alphabets. Extending further, the distributions are significantly different when they are not denoted by the same alphabet or do not share an alphabet in common when denoted by multiple alphabets. For example, in Fig. 3b distributions denoted by 'a' and 'a,e' are not statistically different when compared with each other. However, in pairwise comparisons, both these distributions are significantly different than the distributions denoted by 'b', 'c,d' and 'd'. Further, though distribution denoted by 'a' is different than that denoted by 'c,e', the distribution 'a,e' is not different than the one denoted by 'c,e'. While in most of the cases the difference was considered significant at $P < 0.05$, in two comparisons $P \leq 0.061$ was considered significant and is mentioned as such in the figure legends. SigmaPlot 13.0 was used for statistical analysis using one-way analysis of variance and for plotting box plots.

Binning of microridges into small (0–5 μm), intermediate (5–20 μm), long (20–100 μm) and very long (> 100 μm) categories was done using the frequency function in EXCEL. Microridge frequencies of a given category were expressed as a percentage of the total number of microridges in a cell. The data were plotted against developmental time or genotypes using Microsoft EXCEL. Histograms for comparison of membrane surface area and box and whisker graphs for colocalization coefficients were plotted using Microsoft Excel. Two-tailed Student's *t*-tests for pairwise comparison of means using Microsoft EXCEL was conducted. A significance level of 0.05 was used as cutoff.

Data availability. The authors declare that the data supporting the findings of this study are available within the article and its Supplementary Information files.

References

- Uehara, K., Miyoshi, M. & Miyoshi, S. Cytoskeleton in microridges of the oral mucosal epithelium in the carp, *Cyprinus carpio*. *Anat. Rec.* **230**, 164–168 (1991).
- Bereiter-Hahn, J., Osborn, M., Weber, K. & Voth, M. Filament organization and formation of microridges at the surface of fish epidermis. *J. Ultrastruct. Res.* **69**, 316–330 (1979).
- Centola, G. M. Surface features of exfoliated vaginal epithelial cells during the oestrous cycle of the rat examined by scanning electron microscopy. *J. Anat.* **127**, 553–561 (1978).
- Sharma, A., Anderson, K. I. & Muller, D. J. Actin microridges characterized by laser scanning confocal and atomic force microscopy. *FEBS Lett.* **579**, 2001–2008 (2005).
- Sperry, D. G. & Wassersug, R. J. A proposed function for microridges on epithelial cells. *Anat. Rec.* **185**, 253–257 (1976).
- Laprise, P. & Tepass, U. Novel insights into epithelial polarity proteins in *Drosophila*. *Trends Cell Biol.* **21**, 401–408 (2011).
- Martin-Belmonte, F. & Mostov, K. Regulation of cell polarity during epithelial morphogenesis. *Curr. Opin. Cell Biol.* **20**, 227–234 (2008).
- Betschinger, J., Mechler, K. & Knoblich, J. A. The Par complex directs asymmetric cell division by phosphorylating the cytoskeletal protein Lgl. *Nature* **422**, 326–330 (2003).
- Chalmers, A. D. *et al.* aPKC, Crumbs3 and Lgl2 control apicobasal polarity in early vertebrate development. *Development* **132**, 977–986 (2005).
- Hurov, J. B., Watkins, J. L. & Piwnicka-Worms, H. Atypical PKC phosphorylates PAR-1 kinases to regulate localization and activity. *Curr. Biol.* **14**, 736–741 (2004).
- Müller, H. A. & Wieschaus, E. armadillo, bazooka, and stardust are critical for early stages in formation of the zonula adherens and maintenance of the polarized blastoderm epithelium in *Drosophila*. *J. Cell Biol.* **134**, 149–163 (1996).
- Wodarz, A., Ramrath, A., Grimm, A. & Knust, E. *Drosophila* atypical protein kinase C associates with Bazooka and controls polarity of epithelia and neuroblasts. *J. Cell Biol.* **150**, 1361–1374 (2000).
- Huynh, J. R., Petronczki, M., Knoblich, J. A. & Johnston, St D. Bazooka and PAR-6 are required with PAR-1 for the maintenance of oocyte fate in *Drosophila*. *Curr. Biol.* **11**, 901–906 (2001).
- Cox, D. N., Seyfried, S. A., Jan, L. Y. & Jan, Y. N. Bazooka and atypical protein kinase C are required to regulate oocyte differentiation in the *Drosophila* ovary. *Proc. Natl. Acad. Sci. USA* **98**, 14475–14480 (2001).
- Rolls, M. M., Albertson, R., Shih, H. P., Lee, C. Y. & Doe, C. Q. *Drosophila* aPKC regulates cell polarity and cell proliferation in neuroblasts and epithelia. *J. Cell Biol.* **163**, 1089–1098 (2003).
- Hutterer, A., Betschinger, J., Petronczki, M. & Knoblich, J. A. Sequential roles of Cdc42, Par-6, aPKC, and Lgl in the establishment of epithelial polarity during *Drosophila* embryogenesis. *Dev. Cell* **6**, 845–854 (2004).
- Kim, S. *et al.* Kinase-activity-independent functions of atypical protein kinase C in *Drosophila*. *J. Cell Sci.* **122**, 3759–3771 (2009).
- Bilder, D. & Perrimon, N. Localization of apical epithelial determinants by the basolateral PDZ protein Scribble. *Nature* **403**, 676–680 (2000).
- Lee, C. Y., Robinson, K. J. & Doe, C. Q. Lgl, Pins and aPKC regulate neuroblast self-renewal versus differentiation. *Nature* **439**, 594–598 (2006).
- Klezovitch, O., Fernandez, T. E., Tapscott, S. J. & Vasioukhin, V. Loss of cell polarity causes severe brain dysplasia in Lgl1 knockout mice. *Genes Dev.* **18**, 559–571 (2004).
- Sripathy, S., Lee, M. & Vasioukhin, V. Mammalian Lgl2 is necessary for proper branching morphogenesis during placental development. *Mol. Cell Biol.* **31**, 2920–2933 (2011).
- Sonawane, M. *et al.* Zebrafish penner/lethal giant larvae 2 functions in hemidesmosome formation, maintenance of cellular morphology and growth regulation in the developing basal epidermis. *Development* **132**, 3255–3265 (2005).
- Reischauer, S., Levesque, M. P., Nusslein-Volhard, C. & Sonawane, M. Lgl2 executes its function as a tumor suppressor by regulating ErbB signaling in the zebrafish epidermis. *PLoS Genet.* **5**, e1000720 (2009).
- Sonawane, M., Martin-Maischein, H., Schwarz, H. & Nusslein-Volhard, C. Lgl2 and E-cadherin act antagonistically to regulate hemidesmosome formation during epidermal development in zebrafish. *Development* **136**, 1231–1240 (2009).
- Claudia, S. B., Chris, B. P. & Andrea, H. B. *Drosophila* nonmuscle myosin II promotes the asymmetric segregation of cell fate determinants by cortical exclusion rather than active transport. *Dev. Cell* **5**, 829–840 (2003).
- Peng, C. Y., Manning, L., Albertson, R. & Doe, C. Q. The tumour-suppressor genes *lgl* and *dlg* regulate basal protein targeting in *Drosophila* neuroblasts. *Nature* **408**, 596–600 (2000).
- Lehman, K., Rossi, G., Adamo, J. E. & Brennwald, P. Yeast homologues of tomosyn and lethal giant larvae function in exocytosis and are associated with the plasma membrane SNARE, Sec9. *J. Cell Biol.* **146**, 125–140 (1999).
- Strand, D. *et al.* The *Drosophila* lethal(2)giant larvae tumor suppressor protein forms homo-oligomers and is associated with nonmuscle myosin II heavy chain. *J. Cell Biol.* **127**, 1361–1373 (1994).
- Strand, D., Raska, I. & Mechler, B. M. The *Drosophila* lethal(2)giant larvae tumor suppressor protein is a component of the cytoskeleton. *J. Cell Biol.* **127**, 1345–1360 (1994).
- Dahan, I., Yearim, A., Touboul, Y. & Ravid, S. The tumor suppressor Lgl1 regulates NMII-A cellular distribution and focal adhesion morphology to optimize cell migration. *Mol. Biol. Cell* **23**, 591–601 (2012).
- Kalmes, A., Merdes, G., Neumann, B., Strand, D. & Mechler, B. M. A serine-kinase associated with the p127-(2)gl tumour suppressor of *Drosophila* may regulate the binding of p127 to nonmuscle myosin II heavy chain and the attachment of p127 to the plasma membrane. *J. Cell Sci.* **109**(Pt 6): 1359–1368 (1996).
- Baldwin, R. M. *et al.* Coordination of glioblastoma cell motility by PKC ζ . *Mol. Cancer* **9**, 233 (2010).
- Dahan, I., Petrov, D., Cohen-Kfir, E. & Ravid, S. The tumor suppressor Lgl1 forms discrete complexes with NMII-A and Par6 α -aPKC ζ that are affected by Lgl1 phosphorylation. *J. Cell Sci.* **127**, 295–304 (2014).
- Wan, Q. *et al.* Regulation of myosin activation during cell-cell contact formation by Par3-Lgl antagonism: entosis without matrix detachment. *Mol. Biol. Cell* **23**, 2076–2091 (2012).
- Kaplan, N. A. & Tolwinski, N. S. Spatially defined Dsh-Lgl interaction contributes to directional tissue morphogenesis. *J. Cell Sci.* **123**, 3157–3165 (2010).
- Horne-Badovinac, S. *et al.* Positional cloning of heart and soul reveals multiple roles for PKC lambda in zebrafish organogenesis. *Curr. Biol.* **11**, 1492–1502 (2001).
- Haas, P. & Gilmour, D. Chemokine signaling mediates self-organizing tissue migration in the zebrafish lateral line. *Dev. Cell* **10**, 673–680 (2006).
- Riedl, J. *et al.* Lifeact: a versatile marker to visualize F-actin. *Nat. Methods* **5**, 605–607 (2008).
- Ohshiro, T., Yagami, T., Zhang, C. & Matsuzaki, F. Role of cortical tumour-suppressor proteins in asymmetric division of *Drosophila* neuroblast. *Nature* **408**, 593–596 (2000).
- Plant, P. J. *et al.* A polarity complex of mPar-6 and atypical PKC binds, phosphorylates and regulates mammalian Lgl. *Nat. Cell Biol.* **5**, 301–308 (2003).
- Hoege, C. *et al.* LGL can partition the cortex of one-cell *Caenorhabditis elegans* embryos into two domains. *Curr. Biol.* **20**, 1296–1303 (2010).

42. Clark, B. S. *et al.* Loss of Lgl1 in retinal neuroepithelia reveals links between apical domain size, Notch activity and neurogenesis. *Development* **139**, 1599–1610 (2012).
43. Hava, D. *et al.* Apical membrane maturation and cellular rosette formation during morphogenesis of the zebrafish lateral line. *J. Cell Sci.* **122**, 687–695 (2009).
44. Saotome, I., Curto, M. & McClatchey, A. I. Ezrin is essential for epithelial organization and villus morphogenesis in the developing intestine. *Dev. Cell* **6**, 855–864 (2004).
45. Vicente-Manzanares, M., Ma, X., Adelstein, R. S. & Horwitz, A. R. Non-muscle myosin II takes centre stage in cell adhesion and migration. *Nat. Rev. Mol. Cell Biol.* **10**, 778–790 (2009).
46. Naumanen, P., Lappalainen, P. & Hotulainen, P. Mechanisms of actin stress fibre assembly. *J. Microsc.* **231**, 446–454 (2008).
47. Kovacs, M., Toth, J., Hetenyi, C., Malnasi-Csizmadia, A. & Sellers, J. R. Mechanism of blebbistatin inhibition of myosin II. *J. Biol. Chem.* **279**, 35557–35563 (2004).
48. Chhabra, E. S. & Higgs, H. N. The many faces of actin: matching assembly factors with cellular structures. *Nat. Cell Biol.* **9**, 1110–1121 (2007).
49. Morton, W. M., Ayscough, K. R. & McLaughlin, P. J. Latrunculin alters the actin-monomer subunit interface to prevent polymerization. *Nat. Cell Biol.* **2**, 376–378 (2000).
50. Martijn, G. *et al.* Rap2A links intestinal cell polarity to brush border formation. *Nat. Cell Biol.* **14**, 793–801 (2012).
51. Whiteman, E. L. *et al.* Crumbs3 is essential for proper epithelial development and viability. *Mol. Cell Biol.* **34**, 43–56 (2014).
52. Cui, S., Otten, C., Rohr, S., Abdelilah-Seyfried, S. & Link, B. A. Analysis of aPKClambda and aPKCzeta reveals multiple and redundant functions during vertebrate retinogenesis. *Mol. Cell Neurosci.* **34**, 431–444 (2007).
53. Laprise, P. *et al.* Yurt, Coracle, Neurexin IV and the Na⁺,K⁺-ATPase form a novel group of epithelial polarity proteins. *Nature* **459**, 1141–1145 (2009).
54. Pellikka, M. *et al.* Crumbs, the *Drosophila* homologue of human CRB1/RP12, is essential for photoreceptor morphogenesis. *Nature* **416**, 143–149 (2002).
55. Tanentzapf, G. & Tepass, U. Interactions between the crumbs, lethal giant larvae and bazooka pathways in epithelial polarization. *Nat. Cell Biol.* **5**, 46–52 (2003).
56. Campbell, K., Knust, E. & Skaer, H. Crumbs stabilises epithelial polarity during tissue remodelling. *J. Cell Sci.* **122**, 2604–2612 (2009).
57. Lam, P.-Y., Mangos, S., Green, J. M., Reiser, J. & Huttenlocher, A. *In vivo* imaging and characterization of actin microridges. *PLoS ONE* **10**, e0115639 (2015).
58. Blaser, H. *et al.* Migration of zebrafish primordial germ cells: a role for myosin contraction and cytoplasmic flow. *Dev. Cell* **11**, 613–627 (2006).
59. Wei, Q. & Adelstein, R. S. Conditional expression of a truncated fragment of nonmuscle myosin II-A alters cell shape but not cytokinesis in HeLa cells. *Mol. Biol. Cell* **11**, 3617–3627 (2000).
60. Maître, J.-L. L. *et al.* Adhesion functions in cell sorting by mechanically coupling the cortices of adhering cells. *Science* **338**, 253–256 (2012).
61. Sonal, *et al.* Myosin Vb mediated plasma membrane homeostasis regulates peridermal cell size and maintains tissue homeostasis in the zebrafish epidermis. *PLoS Genet.* **10**, e1004614 (2014).

Acknowledgements

We acknowledge funding support from Wellcome-trust-DBT India alliance (M.S., I.D. and S.B.), DAE-TIFR (Re.R. and M.S.) and CSIR (Ra.R. and C.D.). We thank Professors. Nancy Papalopulu, Erez Raz, C.P. Heisenberg and Soshana Ravid for reagents. Confocal microscopy was done at the imaging facilities in TIFR and IISER-Pune. Prateek Arora and Kirti Gupta helped in confocal imaging. We acknowledge the help from Dr Himanshu Sinha and Prateek Arora for statistical analysis.

Author contributions

Re.R. and M.S. conceived and designed the experiments. Re.R., I.D., Ra.R., S.B. and C.D. performed the experiments. Re.R., I.D., S.B. and M.S. analysed the data. Re.R. and M.S. wrote the paper.

Additional information

Supplementary Information accompanies this paper at <http://www.nature.com/naturecommunications>

Competing financial interests: The authors declare no competing financial interests.

Reprints and permission information is available online at <http://npg.nature.com/reprintsandpermissions/>

How to cite this article: Raman, R. *et al.* aPKC regulates apical localization of Lgl to restrict elongation of microridges in developing zebrafish epidermis. *Nat. Commun.* **7**:11643 doi: 10.1038/ncomms11643. (2016).



This work is licensed under a Creative Commons Attribution 4.0 International License. The images or other third party material in this article are included in the article's Creative Commons license, unless indicated otherwise in the credit line; if the material is not included under the Creative Commons license, users will need to obtain permission from the license holder to reproduce the material. To view a copy of this license, visit <http://creativecommons.org/licenses/by/4.0/>